Chinese Journal of Natural Medicines

Buqi-Tongluo Decoction inhibits osteoclastogenesis and alleviates bone loss in ovariectomized rats by attenuating NFATc1, MAPK, NF-κB signaling

Yongxian Li, Jinbo Yuan, Wei Deng, Haishan Li, Yuewei Lin, Jiamin Yang, Kai Chen, Heng Qiu, Ziyi Wang, Vincent Kuek, Dongping Wang, Zhen Zhang, Bin Mai, Yang Shao, Pan Kang, Qiuli Qin, Jinglan Li, Huizhi Guo, Yanhuai Ma, Danqing Guo, Guoye Mo, Yijing Fang, Renxiang Tan, Chenguang Zhan, Teng Liu, Guoning Gu, Kai Yuan, Yongchao Tang, De Liang, Liangliang Xu, Jiake Xu, Shuncong Zhang

Citation: Yongxian Li, Jinbo Yuan, Wei Deng, Haishan Li, Yuewei Lin, Jiamin Yang, Kai Chen, Heng Qiu, Ziyi Wang, Vincent Kuek, Dongping Wang, Zhen Zhang, Bin Mai, Yang Shao, Pan Kang, Qiuli Qin, Jinglan Li, Huizhi Guo, Yanhuai Ma, Danqing Guo, Guoye Mo, Yijing Fang, Renxiang Tan, Chenguang Zhan, Teng Liu, Guoning Gu, Kai Yuan, Yongchao Tang, De Liang, Liangliang Xu, Jiake Xu, Shuncong Zhang, Buqi-Tongluo Decoction inhibits osteoclastogenesis and alleviates bone loss in ovariectomized rats by attenuating NFATc1, MAPK, NF-κB signaling, Chinese Journal of Natural Medicines, 2025, 23(1), 90-101. doi: 10.1016/S1875-5364(25)60810-7.

View online: https://doi.org/10.1016/S1875-5364(25)60810-7

Related articles that may interest you

Wechat

Chinese Journal of Natural Medicines 23 (2025) 90-101

Contents lists available at ScienceDirect

Chinese Journal of Natural Medicines

journal homepage: www.cjnmcpu.com/

Original article

Buqi-Tongluo Decoction inhibits osteoclastogenesis and alleviates bone loss in ovariectomized rats by attenuating NFATc1, MAPK, NF-κB signaling

Yongxian Li[a,b,c,d,Δ], Jinbo Yuan[d,Δ], Wei Deng[a,b,c,Δ], Haishan Li[a,b,c], Yuewei Lin[a,b,c], Jiamin Yang[a,b,c], Kai Chen[d], Heng Qiu[d], Ziyi Wang[d], Vincent Kuek[d,h], Dongping Wang[a,b,c], Zhen Zhang[a,b,c], Bin Mai[a,b,c], Yang Shao[a,b,c], Pan Kang[a,b,c], Qiuli Qin[a,b,c], Jinglan Li[a,b,c], Huizhi Guo[a,b,c], Yanhuai Ma[a,b,c], Danqing Guo[g], Guoye Mo[b,c], Yijing Fang[b,e], Renxiang Tan[f], Chenguang Zhan[a,b,c], Teng Liu[a,b,c], Guoning Gu[a,b,c], Kai Yuan[b,c], Yongchao Tang[b,c], De Liang[b,c], Liangliang Xu[a,b,c,*], Jiake Xu[d,*], Shuncong Zhang[a,b,c,*]

[a] *The First Clinical Academy, Guangzhou University of Chinese Medicine, Guangzhou 510405, China*
[b] *The First Affiliated Hospital of Guangzhou University of Chinese Medicine, Guangzhou 510407, China*
[c] *Lingnan Medical Research Center of Guangzhou University of Chinese Medicine, Guangzhou 510405, China*
[d] *School of Biomedical Sciences, University of Western Australia, Western Australia 6102, Australia*
[e] *School of Public Health and Management, Guangzhou University of Chinese Medicine, Guangzhou 510405, China*
[f] *The State Key Laboratory of Pharmaceutical Biotechnology, Institute of Functional Biomolecules, Nanjing University, Nanjing 210008, China*
[g] *Foshan Hospital of Traditional Chinese Medicine, Foshan 528000, China*
[h] *Curtin Medical School, Curtin University, Western Australia 6102, Australia*

ARTICLE INFO

Article history:
Received 8 March 2024
Revised 12 May 2024
Accepted 1 June 2024
Available online 20 January 2025

Keywords:
Osteoporosis
Estrogen deficiency
Osteoclast
Buqi-Tongluo
NFATc1
MAPK
NF-κB

ABSTRACT

Osteoporosis is a prevalent skeletal condition characterized by reduced bone mass and strength, leading to increased fragility. Buqi-Tongluo (BQTL) decoction, a traditional Chinese medicine (TCM) prescription, has yet to be fully evaluated for its potential in treating bone diseases such as osteoporosis. To investigate the mechanism by which BQTL decoction inhibits osteoclast differentiation *in vitro* and validate these findings through *in vivo* experiments. We employed MTS assays to assess the potential proliferative or toxic effects of BQTL on bone marrow macrophages (BMMs) at various concentrations. TRAcP experiments were conducted to examine BQTL's impact on osteoclast differentiation. RT-PCR and Western blot analyses were utilized to evaluate the relative expression levels of osteoclast-specific genes and proteins under BQTL stimulation. Finally, *in vivo* experiments were performed using an osteoporosis model to further validate the *in vitro* findings. This study revealed that BQTL suppressed receptor activator of NF-κB ligand (RANKL)-induced osteoclastogenesis and osteoclast resorption activity *in vitro* in a dose-dependent manner without observable cytotoxicity. The inhibitory effects of BQTL on osteoclast formation and function were attributed to the downregulation of NFATc1 and c-fos activity, primarily through attenuation of the MAPK, NF-κB, and Calcineurin signaling pathways. BQTL's inhibitory capacity was further examined *in vivo* using an ovariectomized (OVX) rat model, demonstrating a strong protective effect against bone loss. BQTL may serve as an effective therapeutic TCM for the treatment of postmenopausal osteoporosis and the alleviation of bone loss induced by estrogen deficiency and related conditions.

1. Introduction

Bone undergoes continuous remodeling or turnover, a complex process primarily driven by the coordinated activities of osteoclastic bone resorption and osteoblastic bone formation [1, 2]. Physiological remodeling plays a crucial role in fracture healing, skeletal adaptation to mechanical stimuli, and maintenance of calcium homeostasis [3]. However, pathological remodeling can occur when the balance between bone formation and resorption is disrupted, leading to various bone disorders such as osteoporosis and osteopetrosis [4].

Estrogen plays a crucial role in bone homeostasis, regulating bone mass and strength through its influence on osteoblast and osteoclast activity [5]. It inhibits bone remodeling by directly reducing osteoclastic bone resorption and enhancing osteoblastic bone formation by binding to estrogen receptors [6]. Consequently, estrogen deficiency can lead to increased bone turnover and bone loss. A significant proportion of postmenopausal women experi-

* Corresponding author.
E-mail addresses: xull-2016@gzucm.edu.cn (L. Xu); jiake.xu@uwa.edu.au (J. Xu); spinezsc@126.com (S. Zhang)
Δ These authors contributed equally to this work.

https://doi.org/10.1016/S1875-5364(25)60810-7

ence substantial bone loss or osteoporosis associated with the rapid decline in estrogen levels within 1–2 years after menopause, a condition known as postmenopausal osteoporosis.

Osteoclasts are multinucleated giant cells that function as the primary bone-resorbing cells, playing a crucial role in bone remodeling and calcium homeostasis [7]. These cells are formed through a complex process called osteoclastogenesis, which primarily involves the fusion of mononuclear progenitor cells (precursors) from the monocyte/macrophage lineage. The differentiation of osteoclasts requires the activation of at least three signaling pathways, triggered by several cytokines, including macrophage colony-stimulating factor (M-CSF) and receptor activator of NF-κB ligand (RANKL), along with their associated transcriptional factors or cytokines [8, 9]. M-CSF and rRANKL are the most critical factors and are sufficient to induce the expression of genes that commit circulating osteoclast precursors to form mature osteoclasts. These genes include *Acp5* (encoding tartrate-resistant acid phosphatase, TRAcP), *CTSK* (encoding cathepsin K), *CALCR* (encoding calcitonin receptor), and *ITGB3* (encoding β3-integrin) [10]. M-CSF promotes the survival and proliferation of osteoclast precursors by binding to its sole cell-surface receptor, c-Fms [11]. The binding of M-CSF to c-Fms activates extracellular signal-regulated kinase (ERK) through the phosphorylation of growth factor receptor-bound protein 2 [12, 13]. RANKL is a crucial component of the RANK/RANKL/osteoprotegerin (OPG) signaling pathway. It binds to the surface receptor of osteoclast precursors, RANK, and drives the precursors to commit to osteoclasts, which subsequently express osteoclast phenotypic markers such as calcitonin receptor and TRAcP [14, 15]. Following stimulation with M-CSF and RANKL, the differentiated preosteoclasts fuse to form multinucleated mature osteoclasts, which express mature osteoclast phenotypic markers such as CTSK and MMP9.

Buqi-Tongluo (BQTL) recipe is a traditional Chinese medicine (TCM) prescription comprising several Chinese herbs, including Huangqi (Radix Astragali), Renshen (Radix et Rhizoma Ginseng), Danggui (Radix Angelicae Sinensis), Chuanxiong (Rhizoma Chuanxiong), and Dilong (Pheretima). In TCM theory, BQTL is believed to enhance "Qi-blood" circulation and has been utilized to promote axon regeneration *via* its anti-inflammatory and anti-oxidative properties [16-19]. However, its potential role in preventing bone loss or osteoporosis remains undetermined. This study investigates the effect of BQTL on RANKL-stimulated osteoclastogenesis *in vitro* and verifies its therapeutic role using an osteoporotic ovariectomized (OVX) rat model *in vivo*. Additionally, we examine its underlying mechanisms involved in essential signaling pathways stimulated by RANKL, including MAPK signaling, NF-κB signaling, and calcium signaling.

2. Materials and methods

2.1. Materials, reagents, and antibodies

BQTL capsules were provided by the Guangzhou University of Chinese Medicine (Guangzhou, China) and dissolved in distilled water at a concentration of 30 mg/100 mL for final working dilutions. Fetal bovine serum (FBS) and MEMα (Minimum Essential Medium α) were obtained from Thermo Fisher Scientific Australia (Malaga, WA, Australia). Luciferase assay and MTS assay kits were procured from Promega Corporation (Sydney, NSW, Australia). Primary antibodies against NFATc1 (Cat# sc-7294), c-Fos (Cat# sc-398595), V-ATPase d2 (Cat# sc-517031), integrin-β3 (Cat# sc-21783), CTSK (Cat# sc-48353), ERK (Cat# sc-5294), JNK (Cat# sc-7345), p38 (Cat# sc-81621), IκB-α (Cat# sc-7294), p-ERK (Cat# sc-7383), p-JNK (Cat# sc-6254), p-p38 (Cat# sc-166182), and β-actin (Cat# sc-8432) were sourced from Santa Cruz Biotechnology (Dallas, TX, USA). Primary anti-vinculin antibody (mouse monoclonal) was acquired from solution (Sigma-Aldrich) (Castle Hill, NSW, Australia). Recombinant glutathione *S*-transferase (GST)-rRANKL protein was expressed and purified as previously described [20]. Recombinant human M-CSF was obtained from R&D Systems (Minneapolis, MN, USA). The secondary antibody Alexa 488 Fluor® goat anti-mouse IgG was procured from Thermo Fisher Scientific Australia, while DAPI (4,6-diamidino-2-phenylindole) was sourced from Santa Cruz Biotechnology (Dallas, TX, USA).

2.2. Cell culture and osteoclastogenesis

Fresh bone marrow macrophages (BMMs) were isolated from C57BL/6J mice (6 weeks old) following a protocol approved by the Animal Ethics Committee of the University of Western Australia (RA/3/100/1601). Briefly, fresh bone marrow was extracted from the femur and tibia, then cultured in a complete medium consisting of α-MEM, 10% FBS, penicillin–streptomycin solution (100 units·mL^{-1} and 100 μg·mL^{-1}, respectively), and 50 ng·mL^{-1} M-CSF. Upon reaching full confluence, BMMs were seeded in 96-well plates at a density of 1 × 10^6 cells per well in a complete medium supplemented with 50 ng·mL^{-1} RANKL. The cells were subsequently treated with a series of BQTL dilutions (0.25, 0.5, 0.75, and 1.0 mg·mL^{-1}, respectively) for the designated period. To determine the affected stage of osteoclastogenesis, 1.0 mg·mL^{-1} BQTL was added to the cells in a complete medium and M-CSF. The complete medium was replenished every 2 days, along with fresh GST-rRANKL and BQTL, until multinucleated cells were observed under a light microscope. The cells were then fixed with 2.5% glutaraldehyde for 10 min, washed twice with PBS, and subjected to TRAcP staining. Osteoclasts were identified by positive TRAcP staining and multiple nuclei under a standard light inverted microscope.

2.3. MTS assay for cell viability

BMMs were seeded into 96-well plates (5 × 10^3 cells/well) and cultured overnight. The following day, cells were exposed to various BQTL dilutions (0.25, 0.5, 0.75, 1.0 mg·mL^{-1}, respectively) for 48 h. Upon completion of the incubation period, MTS reagent was added to the cells and incubated at 37 °C for an additional 2 h. The absorbance at 490 nm was measured using a plate reading spectrophotometer (BMG Labtech, Mornington, Australia).

2.4. Visualization of osteoclasts and podosome belts

To visualize podosome belts, BMMs were cultured in 96-well plates (5 × 10^3 cells/well) beneath FBS-coated coverslips (5 mm diameter). The cells were maintained in a complete medium containing 50 ng·mL^{-1} M-CSF. From the second day onward, cells were exposed to GST-rRANKL (50 ng·mL^{-1}) with or without BQTL (0, 0.75, 1.0 mg·mL^{-1}, respectively) for six days, until multinucleated osteoclasts were observed microscopically. Subsequently, osteoclasts were fixed with 4% paraformaldehyde for 10 min and permeabilized with 0.1% Triton X-100 for 10 min. Non-specific binding was blocked using 3% BSA in PBS for 1 h. The cells were then incubated overnight at 4 °C with mouse anti-vinculin antibody (1∶200 dilution), followed by PBS washing. Alexa 488 Fluor® goat anti-mouse IgG secondary antibody was applied to generate green fluorescent signals. The cytoskeletal F-actin belt was labeled with rhodamine phalloidin in darkness for 90 min. After PBS washing, cells were stained with DAPI for 10 min and mounted using ProLong Gold Antifade Mountant (Thermo Fisher Scientific). Podosome belts were visualized using a NIKON A1Si spectral detector confocal system (Nikon Corporation, Tokyo, Japan).

2.5. Hydroxyapatite resorption assay

The function of osteoclasts is crucial for maintaining bone

homeostasis, beyond their formation and morphology [21]. To evaluate BQLT's effect on osteoclast function, we employed a hydroxyapatite resorption assay as previously described [22, 23]. BMMs (1×10^5 cells/well) were seeded in collagen-coated plates (BD Biocoat™, Thermo Fisher Scientific) and incubated in complete *α*MEM with M-CSF. After overnight attachment at 37 °C, cells were stimulated with GST-rRANKL (50 ng·mL^{-1}) until osteoclasts were visible under a light microscope. The cells were then gently harvested using enzyme-free cell dissociation Sigma-Aldrich, counted, and seeded in Corning® Osteo Assay Surface hydroxyapatite-coated plates (Corning, NY, USA) with an equal number of multinucleated cells. These cells were treated with BQLT at various concentrations (0, 0.75, and 1.0 mg·mL^{-1}) in a complete *α*MEM containing M-CSF and GST-rRANKL. After 48 h of culture, half of the hydroxyapatite-coated wells were fixed and stained for TRAcP activity and osteoclast counting. Cells in the remaining wells were washed with 10% bleach, and the hydroxyapatite resorption pit areas were photographed using a Nikon microscope (Nikon Corporation) and quantified with ImageJ software (NIH, Bethesda, MD) [24]. The percentage of hydroxyapatite surface resorbed by osteoclasts was calculated.

2.6. RNA isolation and quantitative real-time PCR (qRT-PCR)

Freshly isolated BMMs from C57BL/6 mice were cultured and seeded in six-well plates (1×10^5 cells/well). BMMs were stimulated with M-CSF and GST-rRANKL without or with BQTL at two concentrations (0.75 and 1.0 mg·mL^{-1}) for 6 days until multinucleated cells were observed. Total RNA extraction from the cells using the TRIzol reagent was performed according to the manufacturer's instructions (Thermo Fisher Scientific). Single-stranded cDNA was reverse transcribed from 1 μg of the total RNA using M-MLV reverse transcriptase with OligoDT primer (Promega, Sydney, NSW, Australia). QRT-PCR was conducted using SYBR Green PCR MasterMix supplied by Thermo Fisher Scientific. The PCR amplification was programmed on a ViiA 7 Real-time PCR thermal cycler (Applied Biosystems, Warrington, Cheshire, UK) as follows: initial denaturation for 10 min at 94 °C, followed by 40 cycles of 15-sec denaturation at 94 °C, annealing for 60 sec at 60 ºC and extension for 2 min at 72 ºC. The specific primers used for PCR reactions are as follows: *C-fos* (Forward: 5'-GCGAGCAACTGAGAAGAC-3'; Reverse: 5'-TTGAAACCCGAGAACATC-3'), *Nfatc1* (Forward: 5'-GGAGAGTCCGAGAATCGAGAT-3'; Reverse: 5'-TTGCAGCTAGGAAGTACGTCT-3'), *Ctsk* (forward: 5'-GGGAGAAAAACCTGAAGC-3'; reverse: 5'-ATTCTGGGGACTCAGAGC-3'), *Acp5* (forward: 5'-TGTGGCCATCTTTATGCT-3'; reverse: 5'-GTCATTTCTTTGGGGCTT-3'), *Actb* (forward: 5'-CACTGTGCCCATCTACGA-3'; reverse: 5'-TGATGTCACGCACGATTT-3'), and *Hprt1* (Forward: 5'-GTTGGGCTTACCTCACTGCT-3'; Reverse: 5'-TAATCACGACGCTGGGACTG-3'). The mRNA expressions of the osteoclast-specific genes (including *C-fos*, *Nfatc1*, *Ctsk*, and *Acp5*) were normalized to the average C_t value of two housekeeping genes (*Actb* and *Hprt1*) using the comparative C_t method ($2^{-\Delta\Delta Ct}$).

2.7. Luciferase reporter assays in vitro

For luciferase reporter assays, the NFATc1 responsive luciferase reporter construct and the NF-*κ*B responsive luciferase reporter construct were stably transfected in RAW264.7 cells (ATCC® TIB-71™, Manassas, VA, USA) [25, 26]. The cells were seeded in 48-well plates overnight at densities of 5×10^4 cells/well and 1.5×10^5 cells/well, respectively. The following day, cells were pretreated with BQTL at various concentrations (0, 0.25, 0.5, 0.75, 1.0 mg·mL^{-1}) for 1 h, then stimulated with 50 ng·mL^{-1} GST-rRANKL for 6 h for NF-*κ*B luciferase assays and 24 h for NFATc1 luciferase assays. After completion, cells were lysed and centrifuged. Luciferase activity was measured and quantified according to the manufacturer's protocol for the Promega Luciferase Assay System (Promega, Sydney, NSW, Australia) using a POLARstar Optima luminescence reader (BMG LABTECH, Ortenberg, Germany) as previously described [23].

2.8. Western blot assay

Freshly isolated BMMs were seeded in 6-well plates (1×10^5 cells/well) and treated with GST-rRANKL (50 ng·mL^{-1}) with or without BQTL for specified durations. Cells were lysed using radiation immune precipitation (RIPA) pyrolysis buffer. Proteins were extracted and separated by SDS-PAGE and transferred to a PVDF membrane (GE Healthcare Life Sciences, Silverwater, NSW, Australia). The membrane was blocked for 1 h with 5% skim milk solution to prevent non-specific binding. Subsequently, membranes were incubated with specific primary antibodies at 4 °C with gentle shaking overnight. The following day, membranes were gently washed three times with PBST, and incubated with appropriate horseradish peroxidase (HRP)-linked secondary antibodies from Thermo Fisher Scientific at room temperature (20 to 25 °C) for 1 h prior to detection. Antibody detection was performed after signal enhancement using the Amersham ECL Prime Western Blot Detection Reagent Kit (GE Healthcare Life Sciences). Digital images of the membranes were captured on an ImageQuant LAS 4000 (GE Healthcare Life Sciences) and analyzed using ImageJ software.

2.9. Ca^{2+} oscillation assay

BMMs were seeded into 48-well plates (1×10^4 cells/well) and cultured under various conditions for 24 h. The negative control group comprised cells cultured with M-CSF (50 ng·mL^{-1}) only. The positive control group included cells stimulated with both GST-rRANKL (50 ng·mL^{-1}) and M-CSF (50 ng·mL^{-1}). The treatment group consisted of cells cultured with the same doses of GST-rRANKL and M-CSF as the positive control group, with the addition of BQTL (1.0 mg·mL^{-1}). Following incubation, the cells were rinsed twice with a HANKS balanced salt solution containing 1% FBS and 1 mmol·L^{-1} probenecid, then stained with a calcium dye (Fluo4, 4 μmol·L^{-1}) in darkness for 50 min. Subsequently, cells were washed with a HANKS-balanced salt solution and incubated in darkness at room temperature for 25 min. Cell fluorescence intensity was visualized using a Nikon A1 laser-scanning fluorescence microscope. Time-lapse images were captured at 2-sec intervals for 3 min. Cells exhibiting oscillations with two or more distinct calcium peaks were identified and counted, and the oscillation intensity was analyzed using the NIS-Elements Basic Research Microscope Imaging Software (Nikon, Tokyo, Japan).

2.10. OVX rat model

Seventeen pathogen-free female rats (Sprague-Dawley) were obtained from the Guangzhou University of Chinese Medicine (Guangzhou, China). The rats were maintained according to the standards for the care and use of experimental animals (Approval No. TCMF1-2018011). They were randomly divided into four groups: sham (n = 3), OVX (n = 6), and two OVX groups treated with different doses of BQTL (n = 4 each). All rats were housed in individually ventilated cages under a 12∶12 h light-dark cycle at 24 °C for 7 days prior to surgery. Surgical procedures were conducted following the protocol described previously [22]. The sham control group underwent a sham-operated procedure, while OVX was performed to create an estrogen-deficient model. Seven days post-OVX procedure, rats in the OVX + BQTL groups were administered BQTL (250 and 500 mg·kg^{-1} as the low and high dose, re-

spectively) every 2 days. The sham and OVX groups received PBS (250 mg·kg^{-1}) on the same schedule. After 6 weeks of treatment, rats were euthanized, and their femurs were collected for micro-computed tomography (μCT) scanning and analysis.

2.11. Micro-CT scanning and analysis

After euthanasia, the hindlimbs were dissected, and the femurs were extracted following the removal of skin and most of the surrounding soft tissues. The femurs were fixed in 10% neutral buffered formalin for 48 h, washed with 1 × PBS for 48 h, and stored in 15 mL tubes containing 70% ethanol for long-term storage. Left femurs were scanned using a μCT scanner (Skyscan 1176, Bruker microCT, Kontich, Belgium). Each scan was conducted under identical conditions: radiation source voltage, 65 kV; source current, 385 μA; aluminum 1.0 mm filter; pixel size 9 μm; and 0.4-degree rotation step through 180°. The raw images for each sample were reconstructed using the accompanying software (NRecon) with consistent settings (ring artifact correction, 7; smoothing, 2; beam hardening correction, 40%; and threshold 0.00–0.06) [23]. A refined region of interest (ROI) for the trabecular bone was selected half mm above the growth plate of the distal femur and 2 mm in height. This ROI was semi-automatically defined by the Skyscan CTAn software and refined with careful manual checks of each slide within the bone compartment, excluding cortical bone. A fixed image threshold (50–255) was applied for binarization to determine trabecular bone. Four essential parameters, as recommended by the American Society for Bone and Mineral Research, including bone volume/total volume (BV/TV), trabecular number (Tb.N), trabecular thickness (Tb.Th), and trabecular separation (Tb.Sp), were analyzed using the program CTAn [27].

2.12. Bone histological preparation and histomorphometric analysis

Following the μCT analysis, the left femurs were individually placed in 15 mL tubes. These tubes were filled with 14% ethylenediaminetetraacetic acid (EDTA) at room temperature, with the EDTA refreshed every two days until the samples were decalcified. The decalcified samples were subsequently embedded in paraffin and sectioned in the sagittal plane to produce high-quality 5 μm thick sections. These sections were then stained with hematoxylin and eosin (H&E) and TRAcP as previously described [22]. The stained sections were scanned using a uScope MXII Digital Microscope Slide Scanner (Microscopes International, Lubbock, TX, USA), and representative images were selected for each sample. Bone histomorphometric analyses were conducted using ImageJ as described previously [28]. While BV/TV was calculated on H&E ROIs, the percentages of osteoclast number/bone surface (N.Oc/BS) and osteoclast surface/bone surface (Oc.S/BS) were calculated on TRAcP ROIs.

2.13. Statistical analysis

All experiments were conducted in triplicate and replicated twice. Data were presented as mean ± standard deviation (SD). Statistical analysis was performed using one-way analysis of variance (ANOVA) followed by a Tukey's Honest Significant Difference (HSD) post-hoc test for multiple group comparisons. A $P < 0.05$ was considered statistically significant.

3. Results

3.1. BQTL alleviates RANKL-induced osteoclastogenesis in vitro

To investigate the impact of BQTL on osteoclastogenesis, freshly isolated BMMs were cultured in 96-well plates and treated with M-CSF and GST-rRANKL in the presence or absence of varying concentrations of BQTL. As shown in Fig. 1A, numerous TRAcP-positive multinucleated osteoclasts formed under GST-rRANKL stimulation, while no such cells were observed in the negative control. BQTL demonstrated a dose-dependent inhibition of osteoclastogenesis. At a concentration of 0.5 mg·mL^{-1}, BQTL exhibited statistically significant suppression of RANKL-induced osteoclastogenesis, with increased inhibition at higher doses. The number of osteoclasts per well decreased proportionally with increasing BQTL concentrations (Fig. 1B). To assess the potential cytotoxicity of BQTL on BMMs, an MTS assay was conducted to evaluate osteoclast viability. BQTL showed no *in vitro* cytotoxic effects on BMMs across the tested concentrations (Fig. 1C). Further investigation into which stage of osteoclastogenesis was affected involved treating BMMs with 1.0 mg·mL^{-1} BQTL at different time points (Figs. 1D and 1E). Results indicated that BQTL impaired osteoclast formation and differentiation throughout all three stages, with the most pronounced effect observed during the early stage (Day 1–3) (Fig. 1F).

To further investigate the impact of BQTL on osteoclast morphology, the cytoskeleton (including podosome belts) and nuclei of the pretreated cells were visualized using rhodamine-phalloidin (red) and anti-vinculin (green). As depicted in Fig. 1G, following GST-rRANKL stimulation, mature osteoclasts in the control group developed characteristic podosome belts and contained at least three nuclei. In contrast, the treatment groups (0.75, 1.0 mg·mL^{-1}) exhibited reduced osteoclast size with fewer nuclei compared to the control group (Figs. 1H and 1I). These observations corroborated the findings from the TRAcP staining mentioned previously.

3.2. BQTL attenuates osteoclastic resorption activity in vitro

We further examined whether BQTL can inhibit osteoclastic resorption activity *in vitro* using hydroxyapatite-coated plates. Mature osteoclasts were treated with various concentrations of BQTL (0, 0.75, 1.0 mg·mL^{-1}) for two days, after which the number of osteoclasts and percentage of resorption area per well were quantified. As illustrated in Figs. 2A and 2B, while smaller osteoclasts were observed in the treatment groups, the number of osteoclasts remained statistically unchanged compared to the BQTL-free group. Nevertheless, the resorption area per osteoclast decreased significantly in the presence of BQTL in a dose-dependent manner, suggesting that BQTL could reduce the resorption activity of osteoclasts (Fig. 2C).

3.3. BQTL attenuates osteoclast-specific gene expression

Several osteoclast-specific genes (e.g., *c-fos*, *Nfatc1*, *Ctsk*, *Acp5*) are significantly upregulated during osteoclast differentiation [29]. This observation provides a basis for investigating the impact of BQTL on the expression of these genes during RANKL-induced osteoclastogenesis using quantitative PCR. The study revealed that these osteoclast-related genes were notably upregulated after GST-rRANKL (50 ng·mL^{-1}) stimulation for 5 days (Fig. 3). However, in the presence of BQTL (0.75 or 1.0 mg·mL^{-1}), the expression levels of these genes were reduced. Collectively, these findings further indicate that BQTL attenuates the expression of osteoclast-specific genes, consistent with its inhibitory effect on osteoclastogenesis *in vitro*.

3.4. BQTL represses NFATc1 activity and protein expression

Subsequently, we examined the potential influence of BQTL on the activity of NFATc1, a key transcription factor in osteoclastogenesis [30]. To achieve this, we performed stable transfection of

RAW264.7 cells with an NFATc1 reporter construct to measure NFATc1 transcriptional activity. As shown in Fig. 4A, NFATc1 activity was significantly upregulated following GST-rRANKL stimulation. However, this activity was notably suppressed by BQTL at doses of 0.75 and 1.0 mg·mL^{-1}. As anticipated, time-course Western blot analysis revealed that NFATc1 expression was attenuated during osteoclast differentiation (Figs. 4B and 4C). The expression of c-fos, a crucial component of AP1, was also found to be inhibited by BQTL at the same time points (Figs. 4B and 4C). Moreover, our results demonstrated that BQTL suppressed the expression of downstream proteins, including V-ATPase-d2, CTSK, and integrin β3, which are associated with osteoclast formation and function, primarily three to five days after BQTL treatment (Figs. 4B and 4C). In summary, BQTL potently inhibits NFATc1 and c-fos activity, as well as the expression of downstream proteins related to osteoclast formation and function.

3.5. BQTL suppresses the RANKL-induced MAPK signaling pathway

We also investigated the role of the MAPK signaling pathway using Western blots. Members of this pathway, including JNK, ERK, and P38, play crucial roles in regulating AP-1 activity [31]. We assessed the phosphorylation of JNK, ERK, and p38 at various time points following GST-rRANKL stimulation. PBS served as a control to evaluate the effect of BQTL (1.0 mg·mL^{-1}) on the phosphorylation of these MAPK members. As illustrated in Figs. 5A and 5B, BQTL significantly reduced the expression levels of p-JNK1/2 in BMMs after 5, 20, and 30 min of co-incubation with GST-rRANKL. Similarly, BQTL suppressed the expression

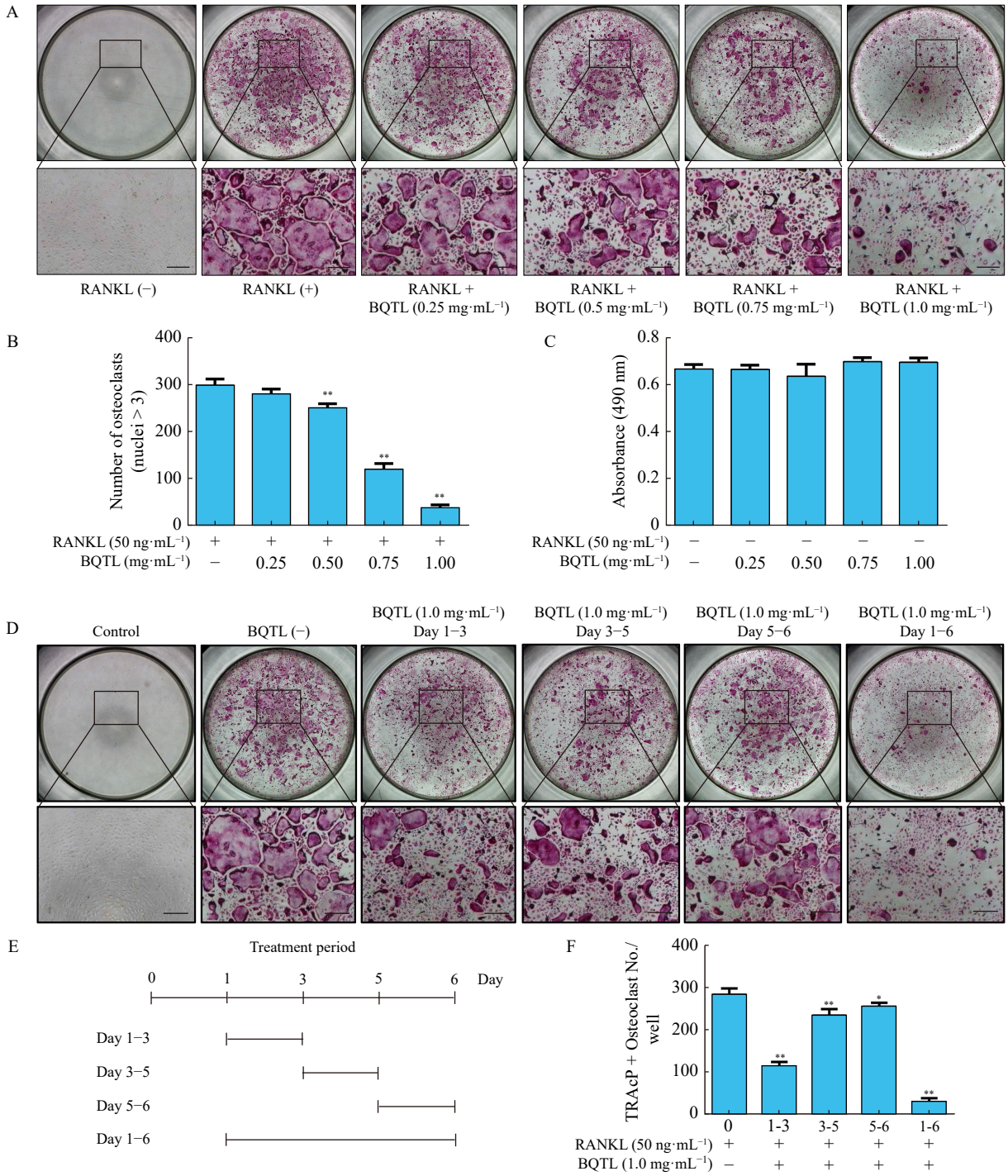

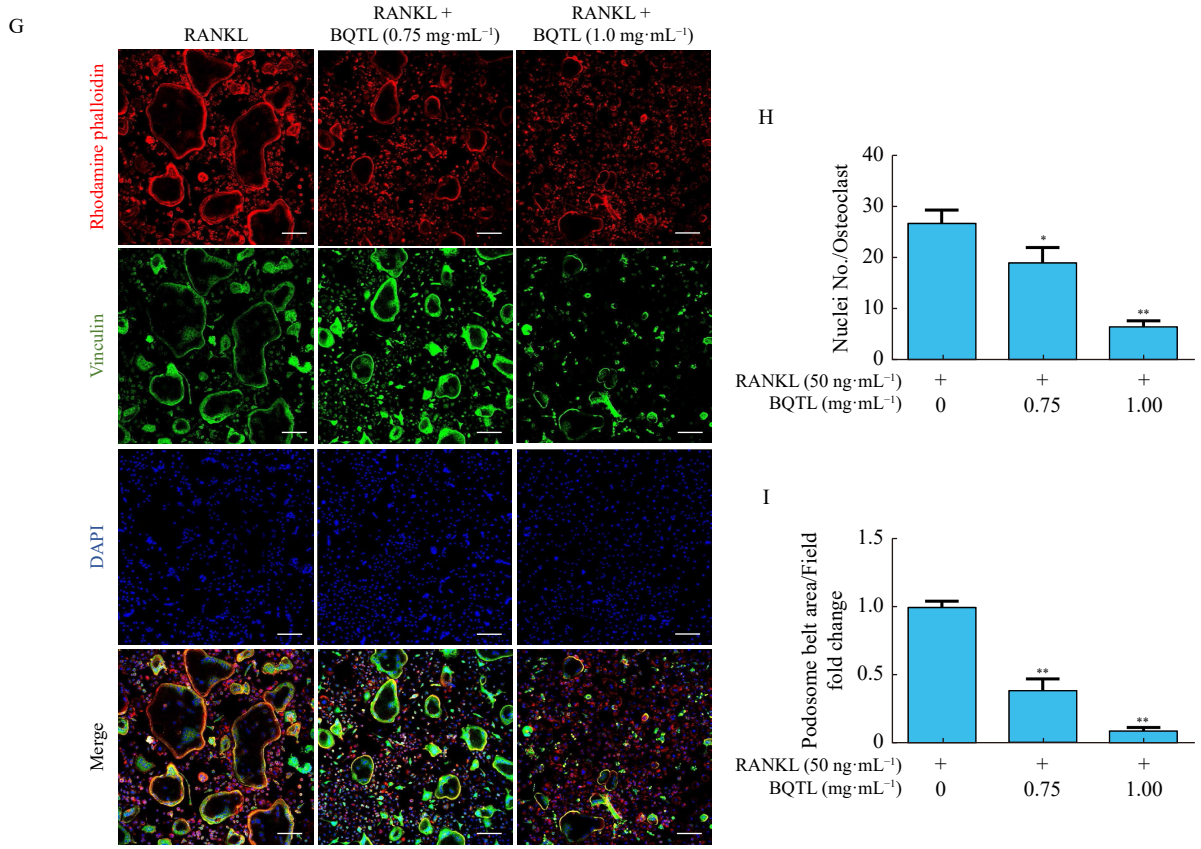

Fig. 1 BQTL alleviates RANKL-induced osteoclastogenesis at an early stage. (A) BQTL affected BMMs in TRAcP staining dose-dependently. (B) TRAcP-positive multinucleated cells (nuclei > 3) were counted per well. (C) Evaluation of BMMs viability 48 h after BQTL treatment using MTS assay. (D) Effects of BQTL (1.0 mg·mL^{-1}) in different periods. The control group contained BMMs stimulated with M-CSF (50 ng·mL^{-1}). Osteoclast formation was induced by M-CSF and GST-rRANKL (each 50 ng·mL^{-1}) and treated with BQTL at various periods. (E) The periods of BQTL treatment. (F) Quantification of TRAcP-positive multinucleated cells (nuclei > 3). (G) Visualization of osteoclasts with podosome belt and nuclei. (H) Number of nuclei per osteoclast. (I) Quantification of podosome belts. Data are represented as mean ± SD (n = 3). The scale bar represents 200 μm. $^{*}P < 0.05$, $^{**}P < 0.01$ *vs* BQTL-free group with GST-rRANKL stimulation.

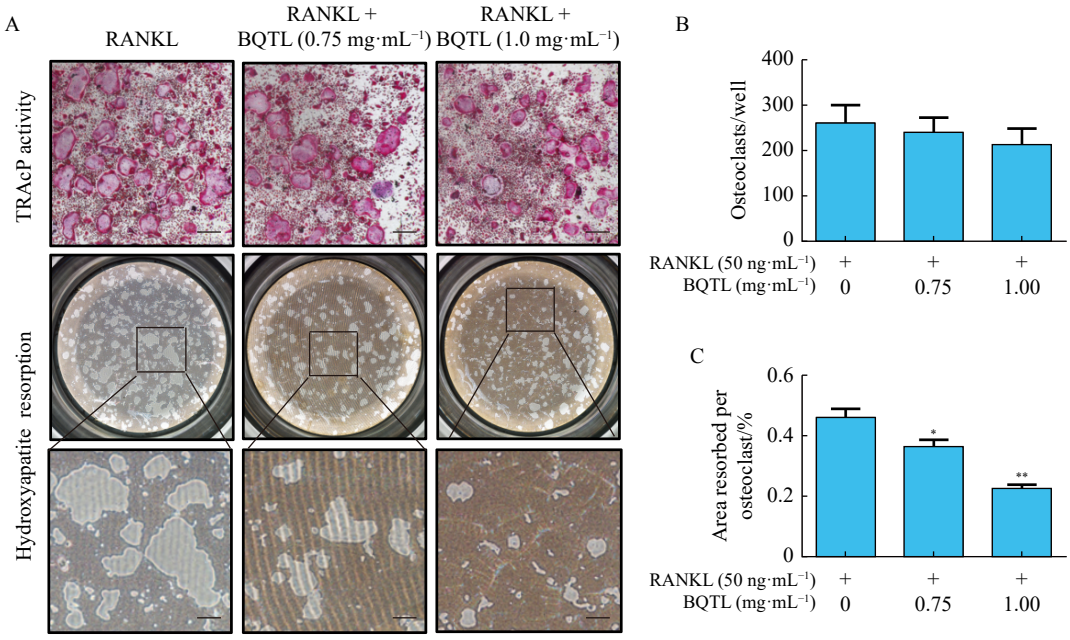

Fig. 2 BQTL attenuates osteoclastic bone resorption. (A) Osteoclastogenesis and hydroxyapatite resorption. BMMs were treated with GST-rRANKL only as control; treatment groups were set with two doses of BQTL (0.75 and 1.0 mg·mL^{-1}, respectively). (B) Quantification of OC number per well. (C) Quantification of hydroxyapatite resorption area per OC. The scale bar represents 200 μm. Data are represented as mean ± SD (n = 3). $^{*}P < 0.05$, $^{**}P < 0.01$ *vs* BQTL-free group.

of p-ERK1/2 from 5 to 30 min after GST-rRANKL stimulation (Figs. 5A and 5C). The inhibitory effect of BQTL on the phosphorylation of P38 was observed across all time points (Figs. 5A and 5D). Collectively, these findings indicate that BQTL strongly downregulates the RANKL-mediated MAPK signaling pathway.

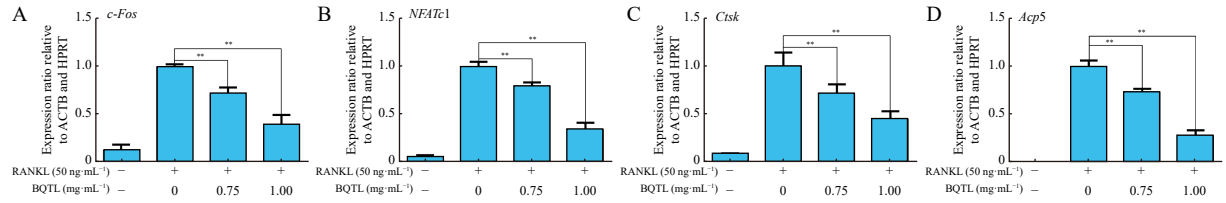

Fig. 3 BQTL attenuates the expression of OC-specific marker genes. The group with BMMs stimulated with M-CSF (50 ng·mL^{-1}) was used as the negative control. The group with BMMs stimulated with GST-rRANKL and M-CSF without BQTL as positive control. Treatment groups were loaded with two designated concentrations of BQTL (0.75 and 1.0 mg·mL^{-1}, respectively). The average expression level of each gene was standardized relative to *ACTB* and *HPRT*. Relative mRNA expression levels during osteoclastogenesis: (A) *NFATc1*, (B) *c-Fos*, (C) *Ctsk*, and (D) *Acp5 (TRAcP)*. Data are represented as mean ± SD (n = 3). $^{*}P < 0.05$, $^{**}P < 0.01$ *vs* BQTL-free group.

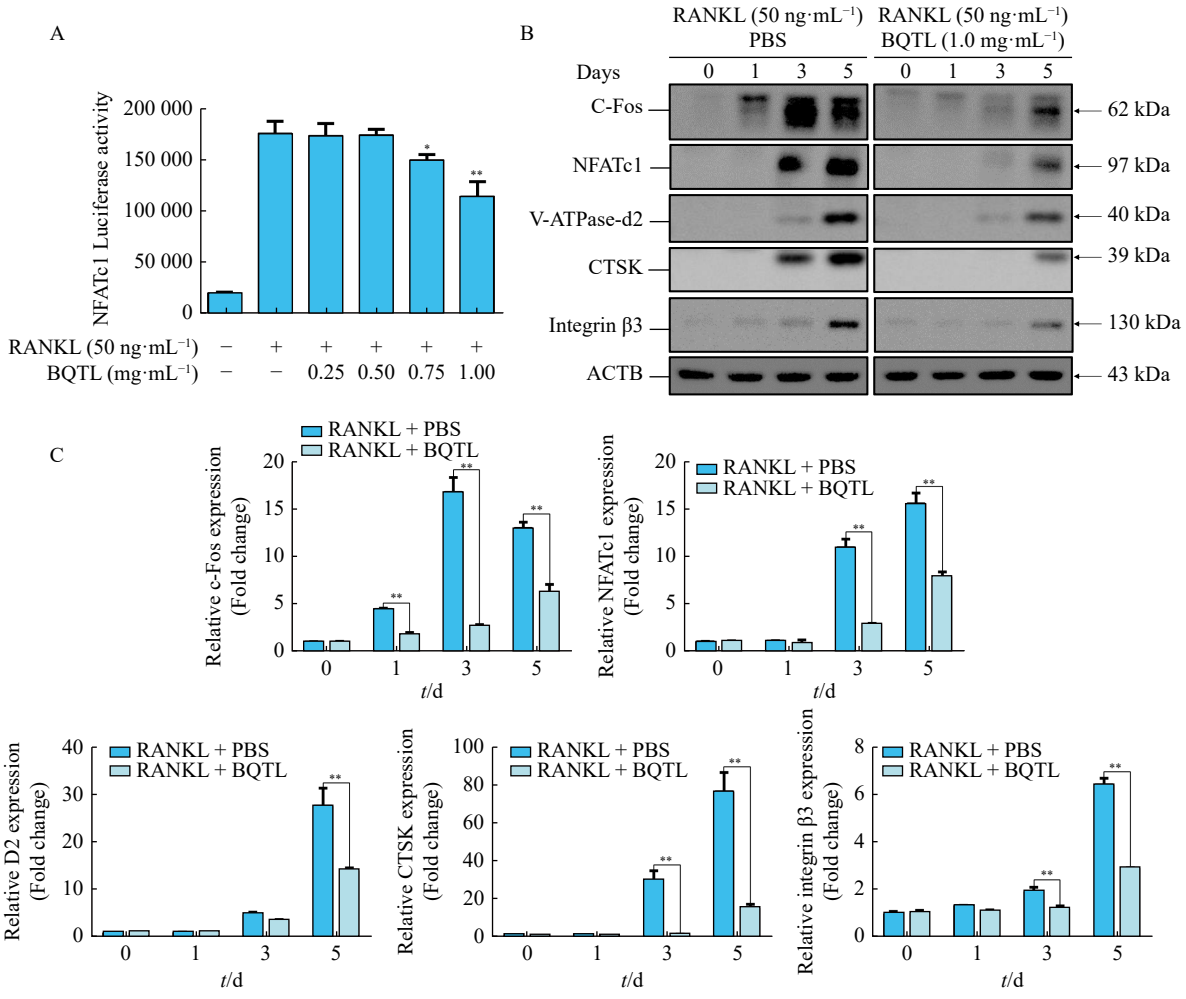

Fig. 4 BQTL represses NFATc1 activity and the expression of downstream proteins. (A) Stable transfection of RAW264.7 cells with the NFATc1 reporter gene construct. Cells were treated with various doses of BQTL. The group with cells plus M-CSF (50 ng·mL^{-1}) was used as the negative control. (B) Expression patterns of c-Fos, NFATc1, Integrin β3, V-ATPase-d2, CTSK, and ACTB at days 0, 1, 3 and 5 after stimulation with M-CSF and GST-rRANKL. PBS (vehicle) was used as control (left column), in comparison to the BQTL treatment group (1.0 mg·mL^{-1}) (right column). (C) Relative quantification of expression patterns relative to ACTB. Data are represented as mean ± SD (n = 3). $^{*}P < 0.05$, $^{**}P < 0.01$ *vs* control.

3.6. BQTL suppresses NF-κB activation and calcium oscillation

The NF-κB pathway is a crucial signaling pathway activated during osteoclastogenesis, with IκB-α serving as the primary signaling molecule associated with NF-κB activation [10]. BQTL treatment at concentrations of 0.75 and 1.0 mg·mL^{-1} was found to diminish NF-κB activity (Fig. 6A). Compared to the GST-rRANKL plus PBS group, BQTL treatment (1.0 mg·mL^{-1}) blocked IκB-α degradation 10–60 min after administration. Additionally, BQTL suppressed the phosphorylation of P65 at 20, 30, and 60 min (Figs. 6B and 6C). Ca^{2+} oscillations, which are induced by RANKL, also contribute to NFATc1 activation [32]. This study examined the intensity of calcium oscillations following GST-rRANKL and/or BQTL treatment. As anticipated, the intensity of calcium oscillations decreased by approximately 40% after the addition of 1 mg·mL^{-1} BQTL (Fig. 7). These results collectively suggest that BQTL could effectively suppress NFATc1 activation, partly due to the inhibition of both GST-rRANKL-induced NF-κB activation and Ca^{2+} oscillations.

3.7. BQTL alleviates estrogen deficiency-induced bone loss

Following the demonstration of BQTL's inhibitory effect on osteoclast formation and function *in vitro*, we assessed its therapeutic potential in treating bone loss or osteoporosis induced by estrogen deficiency using an OVX rat model. Micro-CT analysis revealed that bone mass (primarily indicated by BV/TV) in the OVX rats decreased by approximately 60% compared to the sham

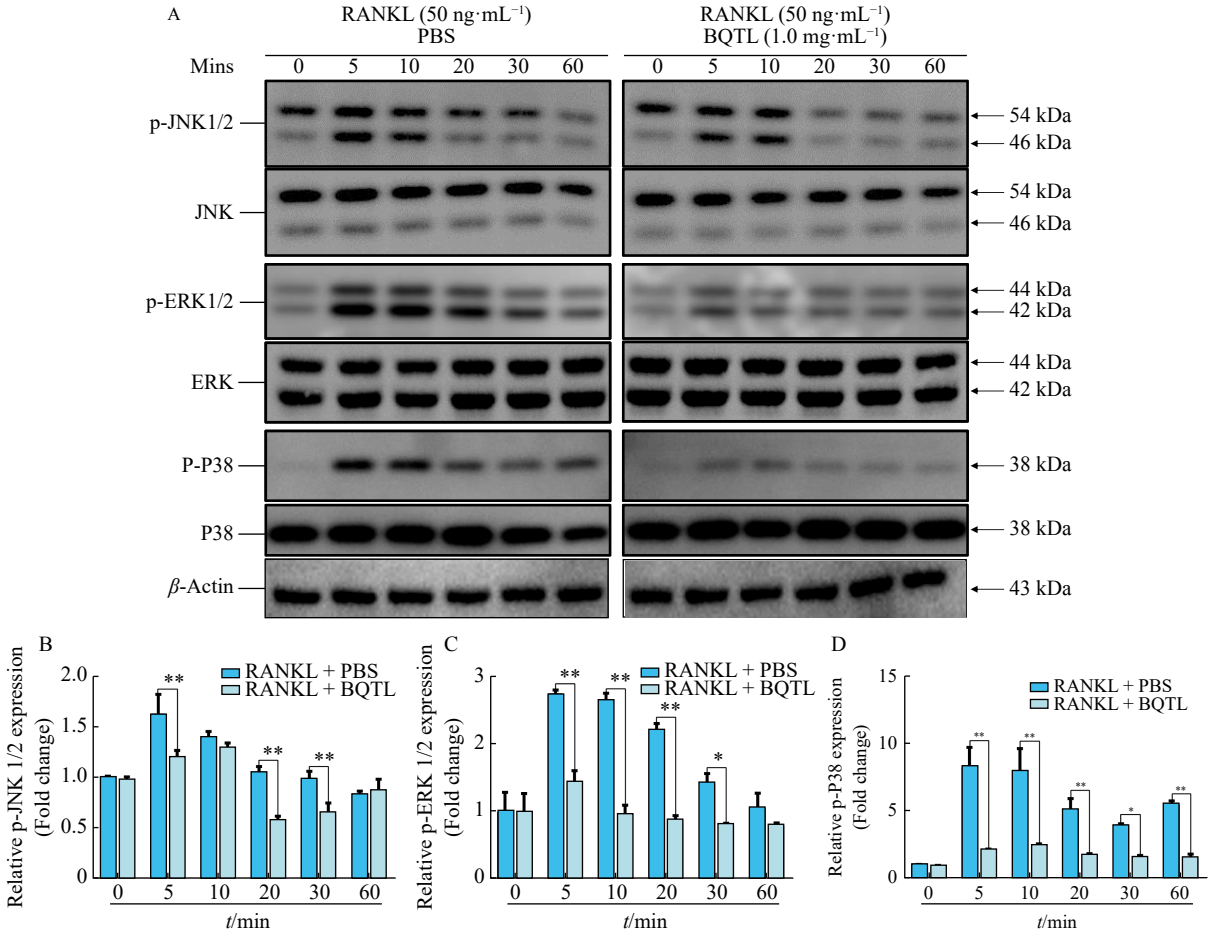

Fig. 5 BQTL suppresses the RANKL-induced MAPK signaling pathway. (A) Expression patterns of p-JNK1/2, JNK, p-ERK1/2, ERK, p-P38, and P38 at 0, 5, 10, 20, 30, 60 min after stimulation with M-CSF and GST-rRANKL. PBS (vehicle) was used as control (left column), in comparison to the BQTL treatment group (1.0 mg·mL^{-1}) (right column). (B–D) The relative ratios of phosphorylated proteins/unphosphorylated proteins. Data are represented as mean ± SD (n = 3). $^{*}P < 0.05$, $^{**}P < 0.01$ *vs* the corresponding PBS control.

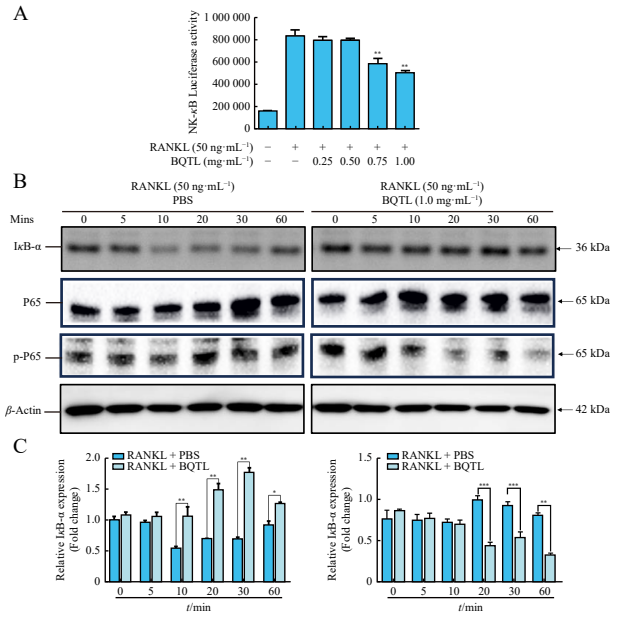

Fig. 6 BQTL suppresses NF-κB activation and IκB-α degradation. (A) Stable transfection of RAW264.7 cells with the NF-κB reporter gene construct. Cells were treated with various doses of BQTL. The group with cells plus M-CSF (50 ng·mL^{-1}) was used as the negative control. (B) Expression patterns of IκB-α and β-actin protein levels of BMMs at a battery of time points after stimulation with M-CSF and GST-rRANKL. PBS (vehicle) was used as control (left column), in comparison to the BQTL treatment group (1.0 mg·mL^{-1}) (right column). (C) Relative protein levels of IκB-α relative to β-actin. Data are represented as mean ± SD (n = 3). $^{*}P <$ 0.05, $^{**}P < 0.01$ *vs* control.

group (Fig. 8), indicating the successful generation of the OVX model. Consistent with our *in vitro* findings, the bone mass was significantly higher in BQTL-treated OVX rats, as evidenced by increased values of BV/TV and Tb.N in a dose-dependent manner. Conversely, the Tb.Sp in BQTL-treated OVX rats was significantly smaller than in OVX rats treated with vehicle (PBS), although no difference was observed between the low- and high-dose groups. Interestingly, Tb.Th, a parameter generally positively correlated with BV/TV and Tb.N, showed no statistically significant difference among all groups.

Histomorphometric analyses further corroborated the μCT findings (Fig. 9). The BV/TV in the OVX group was significantly reduced compared to the sham group. Moreover, BV/TV values increased in OVX rats treated with BQTL, with higher doses corresponding to greater BV/TV values. Conversely, the OVX group exhibited elevated Oc.S/BS and N.Oc/BS compared to the sham group, while these values decreased significantly in the treatment groups in a dose-dependent manner.

4. Discussion

Osteoporosis, the most prevalent skeletal condition, is characterized by reduced bone mass and strength, leading to increased fragility. The incidence of osteoporosis is particularly high in postmenopausal women due to estrogen deficiency and excessive osteoclast activity [33, 34]. This condition has become a major health concern in modern society as the burden of osteoporotic fractures continues to grow. Despite the availability of several classes of drugs for the clinical treatment of osteoporosis,

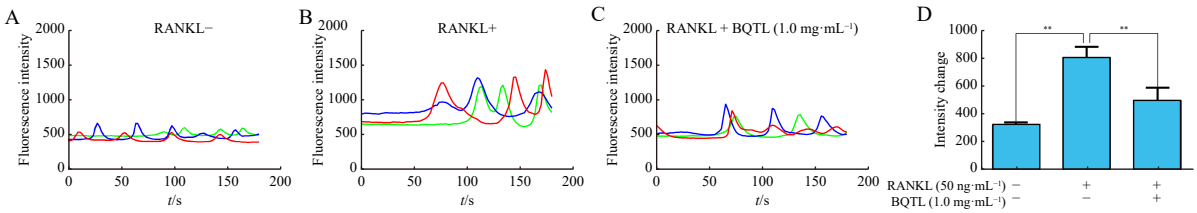

Fig. 7 BQTL suppresses RANKL-induced Ca^{2+} oscillation. (A) Ca^{2+} oscillation patterns with M-CSF only. (B) Ca^{2+} oscillation patterns with M-CSF and GST-rRANKL. (C) Ca^{2+} oscillation patterns of BQTL (1.0 mg·mL^{-1}) after stimulation of M-CSF and GST-rRANKL. (D) Intensity changes of Ca^{2+} oscillation. The intensity changes were calculated as the differences between the highest and the lowest peaks for each group (n = 6). Data are represented as mean ± SD (n = 3). $^{*}P < 0.05$, $^{**}P < 0.01$ *vs* RANKL-induced control.

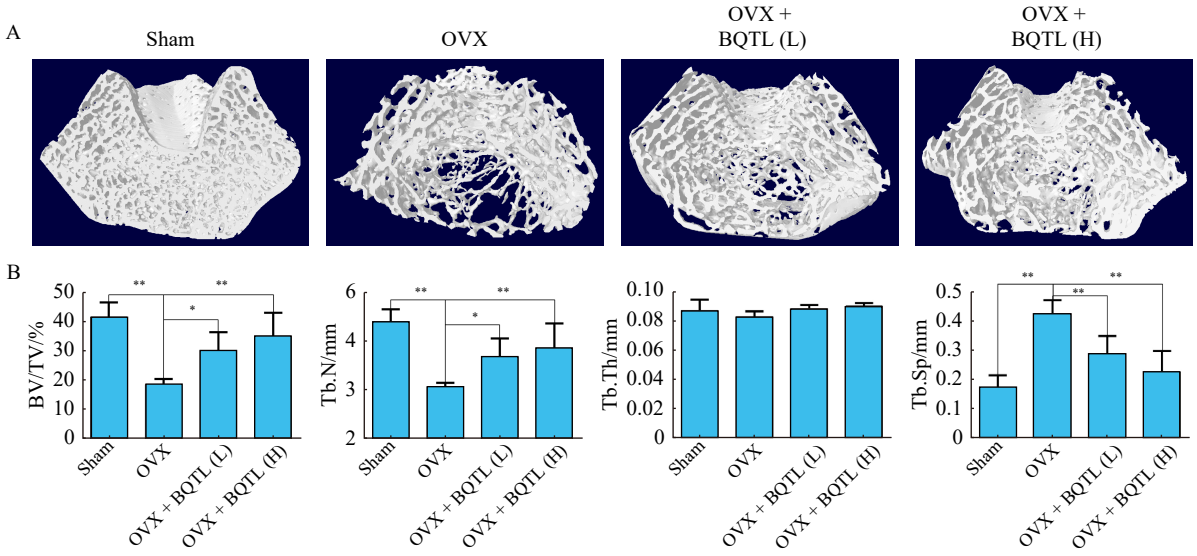

Fig. 8 BQTL alleviates estrogen deficiency-induced bone loss. (A) Trabecular bone mages of distal femurs were dissected from sham, OVX + PBS, and OVX + BQTL groups (low and high, respectively). (B) Quantitative analysis of four essential parameters, including bone volume/total volume (BV/TV), trabecular number (Tb.N), trabecular thickness (Tb.Th), and trabecular separation (Tb.Sp). Data are represented as mean ± SD. $^{*}P < 0.05$, $^{**}P < 0.01$ *vs* OVX + PBS (Sham, n = 3; OVX, n = 6; and OVX groups treated with two different doses of BQTL, n = 4).

there is an urgent need to develop novel therapeutic strategies to address bone loss, given the limited applications and adverse effects of certain existing medications [35, 36]. Considerable research has been directed towards identifying alternative treatments for osteoporosis and related diseases from natural compounds and/or TCM [22, 23, 37]. In this context, we sought to elucidate the mechanisms of BQTL, a potential TCM recipe used for promoting axon regeneration [38], in inhibiting osteoclastogenesis and to verify its potential as a novel alternative treatment for osteoporosis. This study demonstrates that BQTL suppresses osteoclastogenesis *in vitro* and alleviates ovariectomy (OVX)-induced bone loss *in vivo via* the suppression of NFATc1 expression and downregulation of the NF-κB pathway, MAPK pathway, and calcium oscillations (Fig. 10).

The cell-based *in vitro* experiments, including osteoclast culture and hydroxyapatite resorption assay, revealed that BQTL inhibited GST-rRANKL-induced osteoclastogenesis at a concentration of 0.5 mg·mL^{-1} and enhanced its efficacy against osteoclast differentiation at higher doses without compromising cell viability. The results demonstrated that BQTL reduced osteoclast size and the number of nuclei per cell. Both TRAcP staining and immunofluorescence staining showed that BQTL treatment impaired RANKL-induced osteoclastogenesis in a dose-dependent manner. Further investigation indicated that osteoclast formation and differentiation were affected across all three stages, but predominantly during the early stage (Day 1–3) when BMMs were treated with 1.0 mg·mL^{-1}. Notably, no statistically significant difference in osteoclast number was observed among the three groups pretreated with or without BQTL after GST-rRANKL stimulation. These findings suggest that BQTL could mitigate the resorption activity of osteoclasts without altering their quantity.

The downregulation of osteoclast-specific genes (including *c-fos*, *Nfatc1*, *Ctsk*, and *Acp5*) confirms that BQTL inhibits osteoclastogenesis *in vitro* at the transcriptional level. Through the NFATc1 responsive luciferase reporter assay and Western blot analysis, this transcriptional regulator of osteoclastogenesis was found to be significantly repressed by BQTL at both transcriptional and protein expression levels. BQTL, therefore, appears to impair osteoclast differentiation partly *via* suppression of NFATc1 expression. Other osteoclast bone resorption-related proteins, such as V-ATPase-d2, CTSK, and ITGB3 (integrin β3), were also found to be suppressed 3–5 days after BQTL treatment, consistent with findings for several compounds previously reported [23, 37, 39]. These results indicate that BQTL strongly inhibits both NFATc1 and c-fos activity, as well as the downstream protein expression related to osteoclast formation and function.

The MAPK signaling pathway, comprising three key components (JNK, ERK, and P38), has been firmly associated with RANKL-induced osteoclast differentiation *via* the regulation of AP-1 expression [40-42]. Research has demonstrated that phosphorylation of these MAPK components modulates osteoclastogenesis in response to RANKL [43, 44]. Our findings suggest that BQTL significantly decreased the expression levels of p-JNK1/2, p-ERK1/2, and p38, potentially by inhibiting the phosphorylation of these MAPK proteins.

As a transcription factor, NF-κB is present in nearly all nucleated cell types and manifests in various forms [45]. It plays a crucial role in transducing signals during osteoclastogenesis *via* activating its primary signaling molecule, IκB-α, a significant component of the IκB kinase complex [10]. Under normal physiological con-

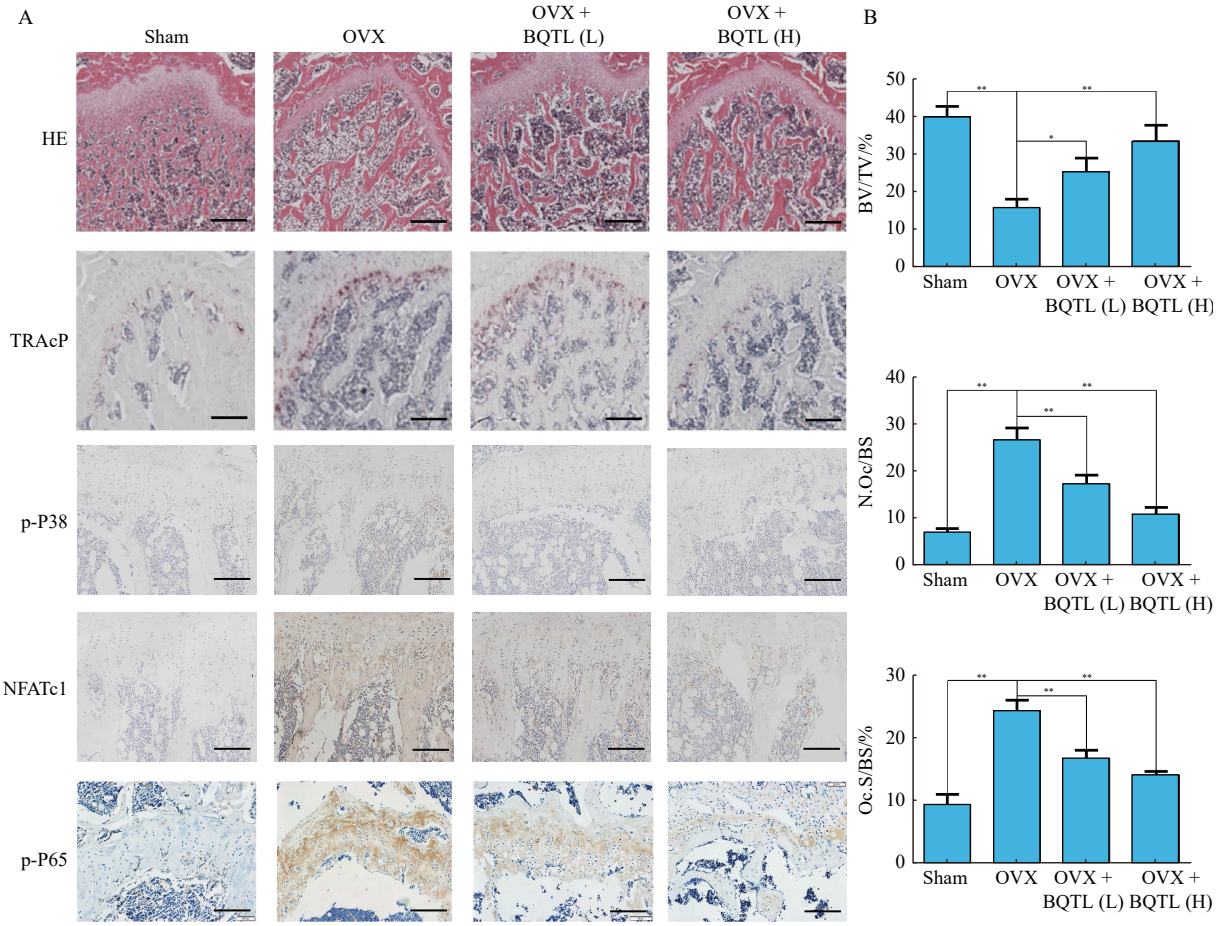

Fig. 9 BQTL alleviates estrogen deficiency-induced bone loss by reducing OC numbers and activity. (A) Representative images of decalcified rat bone stained with H&E, TRAcP, p-P38, NFATc1, and p-P65 from sham, OVX, and OVX rats treated with low and high doses of BQTL. Scale bar = 200 mm. (B) Percentages of bone volume/total volume (BV/TV), OC surface/bone surface (Oc.S/BS), and osteoclast number/bone surface (N.Oc/BS). $^{*}P < 0.05$, $^{**}P < 0.01$ (Sham, $n = 3$; OVX, $n = 6$; and OVX groups treated with two different doses of BQTL, $n = 4$).

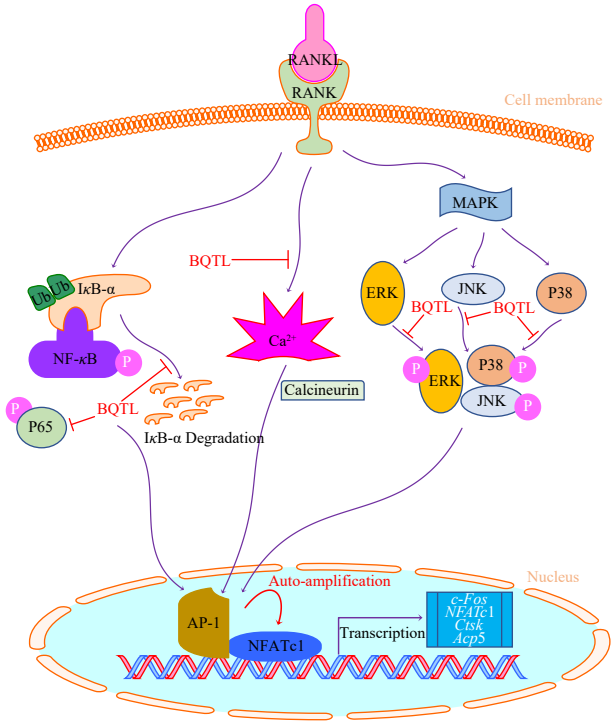

Fig. 10 Proposed scheme for the formation and function of osteoclasts inhibited by BQTL. BQTL attenuates the gene expression of *Acp5*, *c-Fos*, *Nfatc1*, and *Ctsk* by suppressing the MAPK, NF-κB, and calcium signaling pathways and eventually suppressing osteoclast differentiation and function induced by RANKL.

ditions, NF-κB remains in an inactive state bound to IκB [46, 47]. NF-κB is activated in response to various stimuli that induce phosphorylation and degradation of IκB [45]. In its active form, NF-κB translocates to the nucleus, where it activates NFATc1, which subsequently mediates the transcription of osteoclast-specific genes as previously described [30, 48]. Our findings indicate that BQTL not only suppresses the activation of NF-κB but also inhibits the degradation of IκB-α, suggesting BQTL exerts a significant inhibitory effect on osteoclast differentiation, at least partially through suppressing upstream NF-κB signaling. Furthermore, mounting evidence suggests that NFATc1 activation and subsequent auto-amplification are regulated by Ca^{2+} oscillations during RANKL-induced osteoclastogenesis [49, 50]. NFATc1 is thus believed to be mediated by the Ca^{2+}-dependent calcineurin pathway [49]. In conclusion, BQTL appears to suppress the activation of NFATc1 and subsequent osteoclastogenesis likely through its dual roles in selectively inhibiting the NF-κB and Ca^{2+}/calcineurin pathways.

In addition to the compelling results obtained from *in vitro* experiments, an *in vivo* study utilizing an OVX rat model was conducted to assess the efficacy of BQTL in mitigating estrogen-deficiency-induced bone loss. Our findings demonstrated that BQTL exerted a potent protective effect against bone loss in the OVX model. Notably, BQTL did not significantly alter the trabecular thickness among all groups in this study, which aligns with previous research findings. This observation suggests that estrogen deficiency does not markedly affect trabecular thickness, and the regulation of overall trabecular bone mass may differ from that of average trabecular thickness. Furthermore, this study revealed a

strong correlation between μCT and histomorphometric analyses, consistent with our previous report [22, 23, 51].

In conclusion, this study demonstrates the efficacy of BQTL in suppressing RANKL-induced osteoclast formation and function, primarily through the attenuation of MAPK, NF-κB, and Ca^{2+}/calcineurin signaling pathways, consequently leading to the inhibition of NFATc1 and its downstream proteins (Fig. 10). BQTL can not only reduce osteoclast formation and bone resorption function *in vitro* but also mitigate bone loss induced by estrogen deficiency *in vivo*. These findings suggest that BQTL represents a promising therapeutic alternative for the treatment of postmenopausal osteoporosis and the prevention of bone loss associated with estrogen deficiency and related disorders.

Funding

This work was supported by the Natural Science Foundation of Guangdong Province, China (No. 2021A1515012168); the Administration of Traditional Chinese Medicine of Guangdong Province, China (Nos. 20221146 and 20241091); the Basic and Applied Basic Research Fund Project in Guangdong Province, China (No. 2020A1515110948); the Basic and Applied Basic Research in Jointly Funded Projects of City Schools (Institutes) Projects, China (Nos. 202201020500 and 202201020295); the Project of Guangzhou Science and Technology Department, China (No. 202102021040); the Guangzhou Science and Technology Plan Project, China (No. 2023B03J0379); the Chinese Society of Traditional Chinese Medicine Youth Talent Lifting Project (No. 2022-QNRC2-B11); and the Hospital Young and Middle-aged Key Talent Cultivation Project of The First Affiliated Hospital of Guangzhou University of Traditional Chinese Medicine (2023-10).

Ethics approval

The animal experiments were approved by the Animal Ethics Committee of Guangzhou University of Chinese Medicine (approval number: TCMF1-2018011).

Declaration of competing interest

These authors have no conflict of interest to declare.

References

1 Downey PA, Siegel MI. Bone biology and the clinical implications for osteoporosis. *Phys Ther*. 2006;86(1):77–91. https://doi.org/10.1093/ptj/86.1.77.
2 Feehan J, Kassem M, Pignolo RJ, et al. Bone from blood: characteristics and clinical implications of circulating osteogenic progenitor (COP) cells. *J Bone Miner Res*. 2021;36(1):12–23. https://doi.org/10.1002/jbmr.4204.
3 Maciel GB, Maciel RM, Danesi CC. Bone cells and their role in physiological remodeling. *Mol Biol Rep*. 2023;50(3):2857–2863. https://doi.org/10.1007/s11033-022-08190-7.
4 Sobacchi C, Schulz A, Coxon FP, et al. Osteopetrosis: genetics, treatment and new insights into osteoclast function. *Nat Rev Endocrinol*. 2013;9(9):522–536. https://doi.org/10.1038/nrendo.2013.137.
5 Cheng CH, Chen LR, Chen KH. Osteoporosis due to hormone imbalance: an overview of the effects of estrogen deficiency and glucocorticoid overuse on bone turnover. *Int J Mol Sci*. 2022;23(3):1376. https://doi.org/10.3390/ijms23031376.
6 Khalid AB, Krum SA. Estrogen receptors alpha and beta in bone. *Bone*. 2016;87:130–135. https://doi.org/10.1016/j.bone.2016.03.016.
7 Teitelbaum SL. Bone resorption by osteoclasts. *Science*. 2000;289(5484):1504–1508. https://doi.org/10.1126/science.289.5484.1504.
8 Yao Z, Getting SJ, Locke IC. Regulation of TNF-induced osteoclast differentiation. *Cells*. 2021;11(1):132.
9 Chen X, Wang Z, Duan N, et al. Osteoblast-osteoclast interactions. *Connect Tissue Res*. 2018;59(2):99–107. https://doi.org/10.1080/03008207.2017.1290085.
10 Boyle WJ, Simonet WS, Lacey DL. Osteoclast differentiation and activation. *Nature*. 2003;423(6937):337–342. https://doi.org/10.1038/nature01658.
11 Kular J, Tickner J, Chim SM, et al. An overview of the regulation of bone remodelling at the cellular level. *Clin Biochem*. 2012;45(12):863–873. https://doi.org/10.1016/j.clinbiochem.2012.03.021.
12 Zhang XC, Lavoie G, Meant A, et al. Extracellular signal-regulated kinases 1 and 2 phosphorylate Gab2 To promote a negative-feedback loop that attenuates phosphoinositide 3-kinase/Akt signaling. *Mol Cell Biol*. 2017;37(7):e00357–16. https://doi.org/10.1128/MCB.00357-16.
13 Cuevas VD, Simon FM, Orta ZE, et al. The gene signature of activated M-CSF-primed human monocyte-derived macrophages is IL-10-dependent. *J Innate Immun*. 2022;14(3):243–256. https://doi.org/10.1159/000519305.
14 Udagawa N, Koide M, Nakamura M, et al. Osteoclast differentiation by RANKL and OPG signaling pathways. *J Bone Miner Metab*. 2021;39(1):19–26. https://doi.org/10.1007/s00774-020-01162-6.
15 Takayanagi H. RANKL as the master regulator of osteoclast differentiation. *J Bone Miner Metab*. 2021;39(1):13–18. https://doi.org/10.1007/s00774-020-01191-1.
16 Yang ZD, Han QM, He ZH, et al. Effect of Buqi Tongluo prescription on oxygen free radicals in rats with acute crush injury of sciatic nerve. *J Guangzhou Univ Tradit Chin Med*. 2002;4:295–297. https://doi.org/10.13359/j.cnki.gzxbt.cm.2002.04.015.
17 Ding L, Li Y, Yang Y, et al. Wenfei Buqi Tongluo Formula against bleomycin-induced pulmonary fibrosis by inhibiting TGF-beta/Smad3 pathway. *Front Pharmacol*. 2021;12:762998. https://doi.org/10.3389/fphar.2021.762998.
18 Ji Z, Jiang Y, Lin H, et al. Global identification and quantitative analysis of representative components of Xin-Nao-Kang Capsule, a traditional Chinese medicinal formula, by UHPLC-Q-TOF-MS and UHPLC-TQ-MS. *J Pharm Biomed Anal*. 2021;198:114002. https://doi.org/10.1016/j.jpba.2021.114002.
19 Shang H, Zhang K, Guan Z, et al. Optimization of evidence-based research in the prevention and treatment of coronary heart disease with traditional Chinese medicine: a comprehensive review. *J Tradit Chin Med Sci*. 2022;9(2):100–107. https://doi.org/10.1016/j.jtcms.2022.04.004.
20 Xu J, Tan JW, Huang L, et al. Cloning, sequencing, and functional characterization of the rat homologue of receptor activator of NF-kappaB ligand. *J Bone Miner Res*. 2000;15(11):2178–2186. https://doi.org/10.1359/jbmr.2000.15.11.2178.
21 Charles JF, Aliprantis AO. Osteoclasts: more than bone eaters. *Trends Mol Med*. 2014;20(8):449–459. https://doi.org/10.1016/j.molmed.2014.06.001.
22 Zhou L, Liu QL, Yang ML, et al. Dihydroartemisinin, an anti-malaria drug, suppresses estrogen deficiency-induced osteoporosis, osteoclast formation, and RANKL-induced signaling pathways. *J Bone Miner Res*. 2016;31(5):964–974. https://doi.org/10.1002/jbmr.2771.
23 Chen K, Qiu P, Yuan Y, et al. Pseurotin A inhibits osteoclastogenesis and prevents ovariectomized-induced bone loss by suppressing reactive oxygen species. *Theranostics*. 2019;9(6):1634–1650. https://doi.org/10.7150/thno.30206.
24 Schindelin J, Rueden CT, Hiner MC, et al. The ImageJ ecosystem: an open platform for biomedical image analysis. *Mol Reprod Dev*. 2015;82(7-8):518–529. https://doi.org/10.1002/mrd.22489.
25 Wang C, Steer JH, Joyce DA, et al. 12-*O*-tetradecanoylphorbol-13-acetate (TPA) inhibits osteoclastogenesis by suppressing RANKL-induced NF-kappaB activation. *J Bone Miner Res*. 2003;18(12):2159–2168. https://doi.org/10.1359/jbmr.2003.18.12.2159.
26 Cheng JW, Zhou L, Liu Q, et al. Cyanidin chloride inhibits ovariectomy-induced osteoporosis by suppressing RANKL-mediated osteoclastogenesis and associated signaling pathways. *J Cell Physiol*. 2018;233(3):2502–2512. https://doi.org/10.1002/jcp.26126.
27 Bouxsein ML, Boyd SK, Christiansen BA, et al. Guidelines for assessment of bone microstructure in rodents using micro-computed tomography. *J Bone Miner Res*. 2010;25(7):1468–1486. https://doi.org/10.1002/jbmr.141.
28 van't Hof RJ, Rose L, Bassonga E, et al. Open source software for semi-automated histomorphometry of bone resorption and formation parameters. *Bone*. 2017;99:69–79. https://doi.org/10.1016/j.bone.2017.03.051.
29 Asagiri M, Takayanagi H. The molecular understanding of osteoclast differentiation. *Bone*. 2007;40(2):251–264. https://doi.org/10.1016/j.bone.2006.09.023.
30 Kim JH, Kim N. Regulation of NFATc1 in osteoclast differentiation. *J Bone Metab*. 2014;21(4):233–241. https://doi.org/10.11005/jbm.2014.21.4.233.
31 Greenblatt MB, Shim JH, Zou W, et al. The p38 MAPK pathway is essential for skeletogenesis and bone homeostasis in mice. *J Clin Invest*. 2010;120(7):2457–2473. https://doi.org/10.1172/JCI42285.
32 Kuroda Y, Hisatsune C, Nakamura T, et al. Osteoblasts induce Ca^{2+} oscillation-independent NFATc1 activation during osteoclastogenesis. *Proc Natl Acad Sci U S A*. 2008;105(25):8643–8648. https://doi.org/10.1073/pnas.0800642105.
33 Tella SH, Gallagher JC. Prevention and treatment of postmenopausal osteoporosis. *J Steroid Biochem Mol Biol*. 2014;142:155–170. https://doi.org/10.1016/j.jsbmb.2013.09.008.
34 Malle O, Borgstroem F, Fahrleitner PA, et al. Mind the gap: incidence of osteoporosis treatment after an osteoporotic fracture–results of the Austrian branch of the International Costs and Utilities Related to Osteoporotic Fractures Study (ICUROS). *Bone*. 2021;142:115071. https://doi.org/10.1016/j.bone.2019.115071.
35 Rachner TD, Khosla S, Hofbauer LC. Osteoporosis: now and the future. *Lancet*. 2011;377(9773):1276–1287. https://doi.org/10.1016/S0140-6736(10)62349-5.
36 Ishtiaq S, Fogelman I, Hampson G. Treatment of post-menopausal osteoporosis: beyond bisphosphonates. *J Endocrinol Invest*. 2015;38(1):13–29. https://doi.org/10.1007/s40618-014-0152-z.
37 Wang QQ, Yao LY, Xu K, et al. Madecassoside inhibits estrogen deficiency-induced osteoporosis by suppressing RANKL-induced osteoclastogenesis. *J Cell Mol Med*. 2019;23(1):380–394. https://doi.org/10.1111/jcmm.13942.
38 Yao ZS, Liang D. Interventional effect of Buqi Tongluo Fang on the functional recovery of rats after acute crush injury of sciatic nerve. *Chin J Clin Rehab*. 2005;20(2):96–98.
39 Song D, Cao Z, Liu Z, et al. Cistanche deserticola polysaccharide attenuates osteoclastogenesis and bone resorption *via* inhibiting RANKL signaling and

reactive oxygen species production. *J Cell Physiol*. 2018;233(12):9674–9684. https://doi.org/10.1002/jcp.26882.
40 Lee K, Chung YH, Ahn H, et al. Selective regulation of MAPK signaling mediates RANKL-dependent osteoclast differentiation. *Int J Biol Sci*. 2016;12 (2):235–245. https://doi.org/10.7150/ijbs.13814.
41 Peng B, Zhu H, Ma LY, et al. AP-1 transcription factors c-FOS and c-JUN mediate GnRH-induced cadherin-11 expression and trophoblast cell invasion. *Endocrinology*. 2015;156(6):2269–2277. https://doi.org/10.1210/en.2014-1871.
42 Efferth T, Oesch F. The immunosuppressive activity of artemisinin-type drugs towards inflammatory and autoimmune diseases. *Med Res Rev*. 2021;41 (6):3023–3061. https://doi.org/10.1002/med.21842.
43 Lee SE, Woo KM, Kim SY, et al. The phosphatidylinositol 3-kinase, p38, and extracellular signal-regulated kinase pathways are involved in osteoclast differentiation. *Bone*. 2002;30(1):71–77. https://doi.org/10.1016/S8756-3282(01)00657-3.
44 He Y, Staser K, Rhodes SD, et al. Erk1 positively regulates osteoclast differentiation and bone resorptive activity. *PLoS One*. 2011;6(9):e24780. https://doi.org/10.1371/journal.pone.0024780.
45 Wan F, Lenardo MJ. The nuclear signaling of NF-kappaB: current knowledge, new insights, and future perspectives. *Cell Res*. 2010;20(1):24–33. https://doi.org/10.1038/cr.2009.137.
46 Bradford JW, Baldwin AS. IKK/nuclear factor-kappaB and oncogenesis: roles in tumor-initiating cells and in the tumor microenvironment. *Adv Cancer Res*. 2014;121:125–145. https://doi.org/10.1016/B978-0-12-800249-0.00003-2.
47 Boyce BF, Xiu Y, Li JB, et al. NF-kappa B-mediated regulation of osteoclastogenesis. *Endocrinol Metab*. 2015;30(1):35–44. https://doi.org/10.3803/EnM.2015.30.1.35.
48 Asagiri M, Sato K, Usami T, et al. Autoamplification of NFATc1 expression determines its essential role in bone homeostasis. *J Exp Med*. 2005;202(9): 1261–1269. https://doi.org/10.1084/jem.20051150.
49 Negishi KT, Takayanagi H. Ca^{2+}-NFATc1 signaling is an essential axis of osteoclast differentiation. *Immunol Rev*. 2009;231:241–256. https://doi.org/10.1111/j.1600-065X.2009.00821.x.
50 Kuroda Y, Matsuo K. Molecular mechanisms of triggering, amplifying and targeting RANK signaling in osteoclasts. *World J Orthopedics*. 2012;3(11): 167–174. https://doi.org/10.5312/wjo.v3.i11.167.
51 Zhou L, Liu Q, Hong G, et al. Cumambrin A prevents OVX-induced osteoporosis *via* the inhibition of osteoclastogenesis, bone resorption, and RANKL signaling pathways. *FASEB J*. 2019;33(6):6726–6735. https://doi.org/10.1096/fj.201800883RRR.